Compact superconducting single- and dual-band filter design using multimode stepped-impedance resonator*

Xiang Wang(王翔)[1], Bin Wei(魏斌)[1,†], Xi-Long Lu(陆喜龙)[2]
Xu-Bo Guo(郭旭波)[1], and Bi-Song Cao(曹必松)[1]

[1] *State Key Laboratory of Low-Dimensional Quantum Physics, Department of Physics, Tsinghua University, Beijing* 100084, *China*
[2] *The No.* 14 *research institute, China Electronic Technology Corporation (CETC), Nanjing* 210013, *China*

(Received 20 July 2017; revised manuscript received 18 August 2017; published online 20 October 2017)

This study presents two multimode stepped-impedance structures to design single- and dual-band filters. Transmission zeroes are introduced for the single-band filter by using dual-mode stepped-impedance resonators. The single-band filter with high selectivity is centered at 6.02 GHz and has a fractional bandwidth (FBW) of 25.6%. Four stubs (two low frequency and two high frequency ones) are connected to the rectangular patch in the center to construct a quadruple-mode resonator. The independent conditions of the center frequencies of the high and low bands of the resonator are analyzed. A dual-band filter, which operates at 1.53 GHz and 2.44 GHz with FWBs of 12.1% and 14.1%, respectively is designed. The single- and dual-band filters are both fabricated with double-sided YBCO films and they can be used in mobile and satellite communications.

Keywords: high-temperature superconducting, bandpass filter, multimode stepped-impedance resonator, dual-band filter

PACS: 85.25.–j **DOI:** 10.1088/1674-1056/26/12/128501

1. Introduction

The rapid development of wireless technologies leads to increasing demands for single- and dual-band microwave components such as band-pass filters.[1–8] It is well known that with significantly low surface resistance, high-temperature superconducting (HTS) thin films can be used for HTS filters[9,10] for low loss and high out-of-band rejection.

Extensive studies have been carried out to realize single- and dual-band band-pass filters. A cascade quadruplet coupling structure[11,12] was used to generate transmission zeros for the high out-of-band rejection characteristics of a single-band filter. This method requires at least four resonators to realize the coupling structure. In Ref. [13], a novel microstrip feedline structure was used to introduce an extra and controllable transmission zero. This method does not need to change the main structure of the filter. However, the reconfigurable capacitor structure will cause a bad influence on the insertion loss. A dual-band filter, which was implemented by stepped-impedance resonators (SIRs) with a frequency mapping approach, was previously presented.[14] A two-pole dual-wideband filter was also designed by using short-circuited SIRs with controllable center frequencies and bandwidths.[15] A stub-loaded SIR was proposed in the design of dual-band filters,[16] which exhibited multiple tunable transmission zeroes and transmission poles. However, the SIR dimensions significantly affected frequencies, and controlling the two bands independently by using the SIRs was difficult. Moreover, a superconducting dual-band filter that utilized stub-loaded resonators (SLRs) was presented in Ref. [17]. However, the two passband center frequencies were interdependent, thereby affecting the efficiency of the filter design. A multimode resonator(MMR)[18] was applied to a compact-size dual-band filter. Each MMR could be independently designed for one passband. But the short-ended via could hardly apply to the substrate of superconducting material. Thus far, designing dual-band filters with compact circuit size and low insert loss is still a challenge.

In the present work, a traditional dual-mode stepped-impedance resonator (DSIR) is used for a six-pole single-band filter with high out-of-band rejection. With the coupling between the different modes of the two DSIRs, two transmission zeroes are introduced besides the two sides of the passband. Moreover, a novel quadruple-mode stepped-impedance resonator (QSIR) is proposed, and the high- and low-band frequencies are independent and controllable. The QSIR independent conditions of center frequencies of two bands are analyzed. A compact dual-band filter with good performance is designed and fabricated. These filters can be used in the mobile communication.

*Project supported by the National Natural Science Foundation of China (Grant No. 61371009) and the Fund from the Chinese Ministry of Science and Technology (Grant No. 2014AA032703).

†Corresponding author. E-mail: weibin@mail.tsinghuaedu.cn

© 2017 Chinese Physical Society and IOP Publishing Ltd

2. Single-band bandpass filter design

A traditional dual-mode stepped-impedance resonator (DSIR) shown in Fig. 1(a) is used for designing the high selective single-band through introducing controllable transmission zeroes. The DSIR is composed of two high-impedance parts and a low-impedance part. Using the odd- and even-mode method,[19] the structure exhibits an odd- and an even-mode resonance when the symmetrical plane is set at an electric wall (Fig. 1(b)) and a magnetic wall (Fig. 1(c)), respectively. Thus it acts as a non-degenerate dual-mode resonator. The even- and odd-mode resonant frequencies can be calculated using Eqs. (1) and (2).

$$Y_{\mathrm{ine}} = Y_{\mathrm{a}} \frac{Y_{\mathrm{e}} + \mathrm{j}Y_{\mathrm{a}} \tan\theta_{\mathrm{a}}}{Y_{\mathrm{a}} + \mathrm{j}Y_{\mathrm{e}} \tan\theta_{\mathrm{a}}} \frac{Y_{\mathrm{b}}}{Y_{\mathrm{a}}} = \frac{\tan\theta_{\mathrm{a}}}{\cot(\theta_{\mathrm{c}}/2)}, \tag{1}$$

$$Y_{\mathrm{ino}} = Y_{\mathrm{a}} \frac{Y_{\mathrm{o}} + \mathrm{j}Y_{\mathrm{a}} \tan\theta_{\mathrm{a}}}{Y_{\mathrm{a}} + \mathrm{j}Y_{\mathrm{o}} \tan\theta_{\mathrm{a}}} \frac{Y_{\mathrm{c}}}{Y_{\mathrm{a}}} = \frac{\tan\theta_{\mathrm{a}}}{\tan(\theta_{\mathrm{b}}/2)}. \tag{2}$$

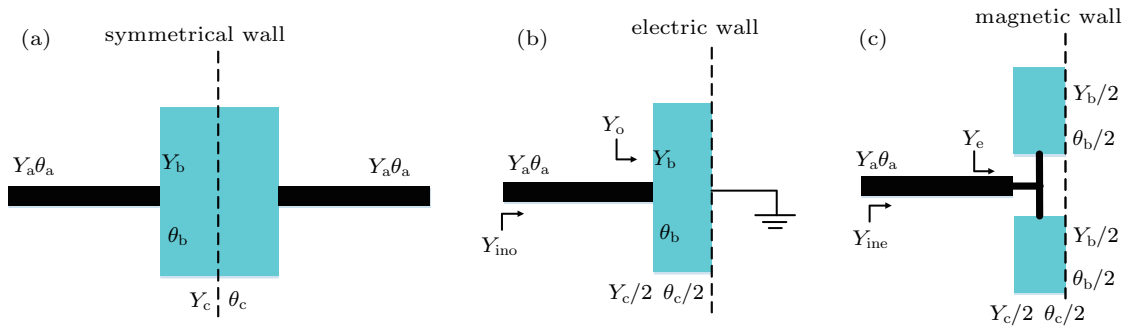


Fig. 1. (color online) (a) Traditional dual-mode stepped-impedance structure. (b) Odd-mode circuit of dual-mode structure. (c) Even-mode circuit dual-mode structure.

Notably, no coupling occurs between the two modes of the dual-mode resonator. According to the theory of asynchronously tuned coupled resonators,[20] if the mode-split frequencies are equal to the self-resonant frequencies, respectively, then no coupling occurs between the two modes. The two split-mode frequencies can be verified by a full-wave electromagnetic (EM) simulation no matter whether they are equal to the two self-resonant frequencies, which can be obtained from Eqs. (1) and (2). Another distinct characteristic is that when two DSIRs are coupled by parallel lines, couplings exists between the same modes (i.e., the even-mode of dual-mode resonator 1 and that of dual-band resonator 2), and between different modes (i.e., the even-mode of dual-mode resonator 1 and the odd-mode of dual-mode resonator 2). Moreover, the two types of couplings have the opposite signs (i.e., the couplings between the same modes have positive signs, whereas the couplings between the different modes have negative signs), and two transmission zeroes are observed in this coupling structure. In order to demonstrate it, a six-pole single-band filter with two dual-mode resonators is designed as shown in Fig. 2(a). The overall circuit size of this filter is 25.00 mm×6.00 mm and its coupling structure is shown in Fig. 2(b). Nodes 2 and 3 represent the odd- and even-mode of a dual-mode resonator, whereas Nodes 4 and 5 are the odd- and even-mode of the other dual-mode resonator, respectively. The solid lines indicate positive couplings between the same modes and the broken lines denote the negative couplings between different modes. The external feedlines are properly adjusted to generate another two resonators, which are denoted as Nodes 1 and 6. This filter is centered at 6.02 GHz with a fractional bandwidth (FBW) of 25.7% and the matrix can be expresses as follows:

$$[m] = \begin{bmatrix} 0 & 0.1499 & 0.1422 & 0 & 0 & 0 \\ 0.1499 & 0.1266 & 0 & 0.07497 & -0.07755 & 0 \\ 0.1422 & 0 & -0.167 & -0.07755 & 0.07238 & 0 \\ 0 & 0.07497 & -0.07755 & 0.1266 & 0 & 0.1499 \\ 0 & -0.07755 & 0.07238 & 0 & -0.167 & 0.1422 \\ 0 & 0 & 0 & 0.1499 & 0.1422 & 0 \end{bmatrix}. \tag{3}$$

The non-zero diagonal elements (i.e., m_{22} and m_{44}, m_{33}, and m_{55}) can be used to extract the resonant frequencies in association with the odd- and even-modes, respectively, and the external quality factor is 4.13. Small differences are observed between the matrix elements and the coupling coefficients are extracted from the filter topologies, because when the filter FBW $>$ 20%, couplings are strongly frequency dependent. The theoretical and simulated performances of the filter are shown in Fig. 3. The whole simulation is based on a lossless transmission line model. Two transmission zeroes are ob-

served on the two sides of the passband.

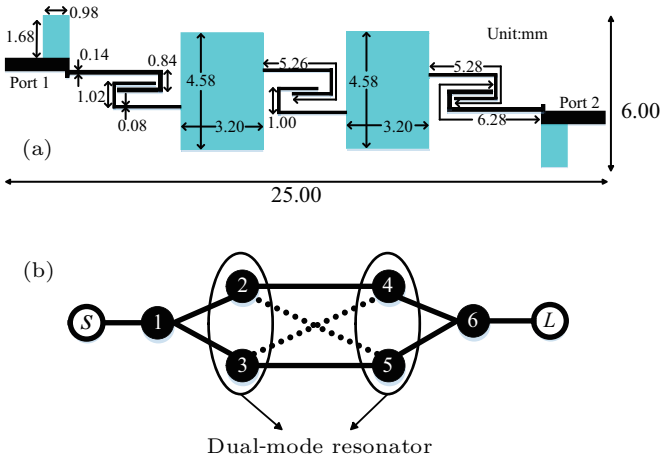


Fig. 2. (color online) (a) Six-pole single-band filter and (b) its coupling structure.

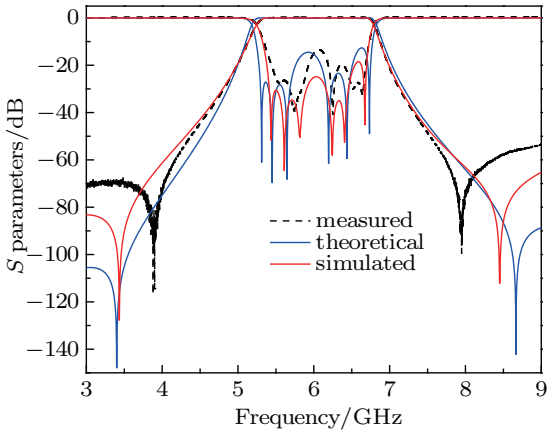


Fig. 3. (color online) Theoretical, simulated, and measured single-band filter performance.

3. Dual-band bandpass filter design

Based on the dual-mode stepped-impedance structure, two stubs are added to form a quadruple-mode stepped-impedance resonator (QSIR) as shown in Fig. 4(a). It features two pairs of high-impedance stubs connected to a central patch. This structure can be used for a dual-band filter design. One pair is for high-band, and the other pair is for low-band. This structure has a horizontal and vertical symmetrical plane (the broken lines in Fig. 4(a)). Under the even- or odd-mode excitations, the vertical plane behaves as a perfect magnetic wall or an electric wall. For the horizontal band, the odd- and even- mode equivalent circuits of the quadruple-mode resonator are shown in Figs. 4(b) and 4(c), respectively. The odd-mode input admittance $Y_{\text{in-odd}}$ can be derived as

$$Y_{\text{in-odd}} = -\mathrm{j}Y_2 \frac{Y_y - Y_2 \tan\theta_2 \tan\theta_x}{Y_2 \tan\theta_x + Y_y \tan\theta_2}. \tag{4}$$

$Y_{\text{in-odd}} = 0$ shows that the resonance condition of the odd-mode has nothing to do with the vertical stubs. Meanwhile, the odd-mode input admittance $Y_{\text{in-even}}$ can be obtained as follows:

$$Y_{\text{in2}} = 2\mathrm{j}Y_x \frac{Y_1 \tan\theta_1 + Y_x \tan\theta_y}{Y_x - Y_1 \tan\theta_1 \tan\theta_y}, \tag{5}$$

$$Y_{\text{in-even}} = Y_2 \frac{Y_{\text{in2}} + Y_2 \tan\theta_2}{Y_2 + \mathrm{j}Y_{\text{in2}} \tan\theta_2}. \tag{6}$$

We define $K_1 = Y_1/Y_x$. If $K_1 \ll 1$, then Eqs. (5) and (6) yield

$$Y_{\text{in2}} = 2\mathrm{j}Y_x \frac{K_1 \tan\theta_1 + \tan\theta_y}{1 - K_1 \tan\theta_1 \tan\theta_y} \approx 2\mathrm{j}Y_x \tan\theta_y, \tag{7}$$

$$Y_{\text{in-even}} = \mathrm{j}Y_2 \frac{2Y_x \tan\theta_y + Y_2 \tan\theta_2}{Y_2 - 2Y_x \tan\theta_y \tan\theta_2}. \tag{8}$$

Equation (8) indicates that the even-mode resonance condition of the horizontal band, $Y_{\text{in-even}} = 0$ is unrelated to the vertical stubs. Analogously, we define $K_2 = Y_2/Y_y$. If $K_2 \ll 1$ is satisfied, then the resonance condition of the vertical band is irrelevant to the horizontal stubs. In summary, the independent conditions of the center frequencies of the high and low bands of the QSIR are $K_1 \ll 1$ and $K_2 \ll 1$. This conclusion demonstrates that to make one band less influenced by the other band, widths w_1 and w_2 should be sufficiently small compared with the length and width of the patch.

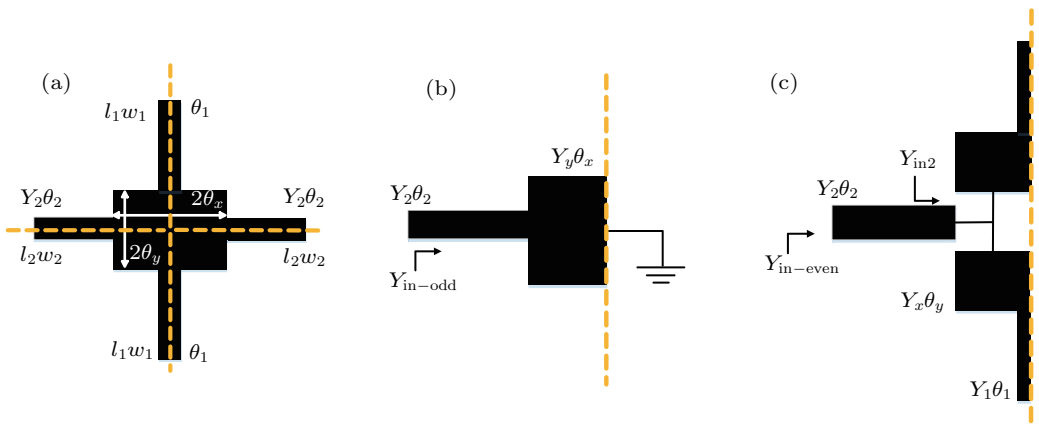


Fig. 4. (color online) (a) Quadruple-mode stepped-impedance structure and its symmetrical planes. (b) Odd-mode circuit of QSIR when a vertical plane is applied. (c) Even-mode circuit of QSIR when a vertical plane is applied.

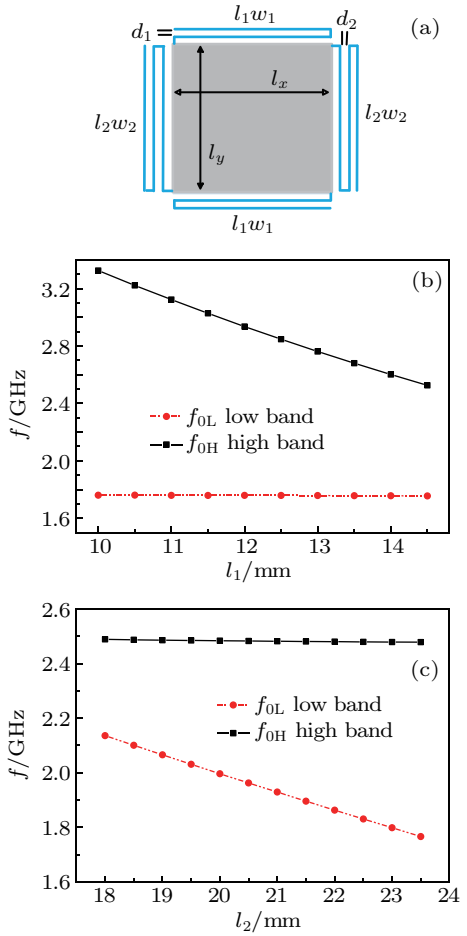


Fig. 5. (color online) (a) Quadruple-mode stepped-impedance resonator. (b) Center frequencies versus l_1, with l_2 fixed at 23.66 mm. (c) Center frequencies versus l_2 with l_1 fixed at 14.82 mm.

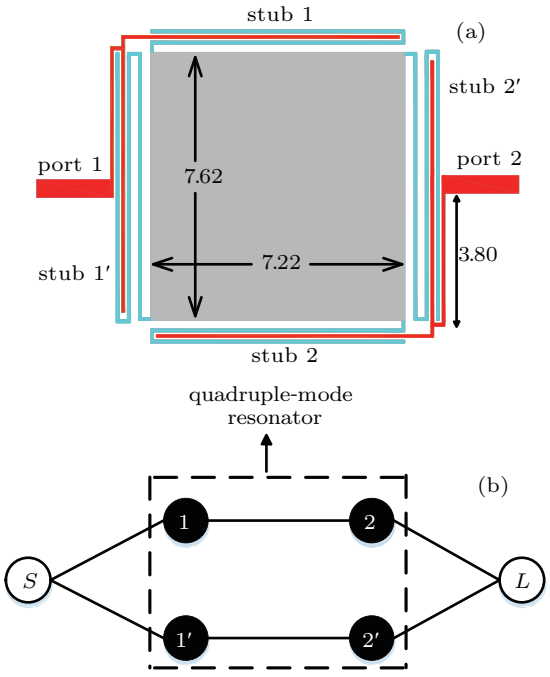


Fig. 6. (color online) (a) Layout and (b) coupling structure of the dual-band filter by using the quadruple-mode stepped-impedance resonator.

In this study, only one QSIR is used to design a dual-band filter and all the stubs are folded for a compact size. The QSIR is shown in Fig. 5(a), and its physical dimensions are listed in Table 1. In comparison with l_x and l_y, widths w_1 and w_2 are quite small to satisfy the independent conditions mentioned above. All stubs are connected to the corners of the patch for flexibility and freedom. The center frequencies of the high and low bands are still independent as shown in Figs. 5(b) and 5(c). When l_1 (high-band stub length of the QSIR in Fig. 5(a)) increases (l_2 is fixed), f_{0H} (center frequency of the low band) decreases, while f_{0L} remains unchanged. When l_2 increases (l_1 is fixed), f_{0L} decreases and f_{0H} remains unchanged. For this structure, when the high-band frequency decreases by 31.67%, the frequency of the low band resonator is slightly affected and decreases only by 0.27% due to simulation in Fig. 5(b).

Table 1. Dimensions (millimeter) in Fig. 5(a).

l_1	l_2	l_x	l_y	w_1	w_2	d_1	d_2
14.82	23.66	7.22	7.62	0.08	0.08	0.24	0.24

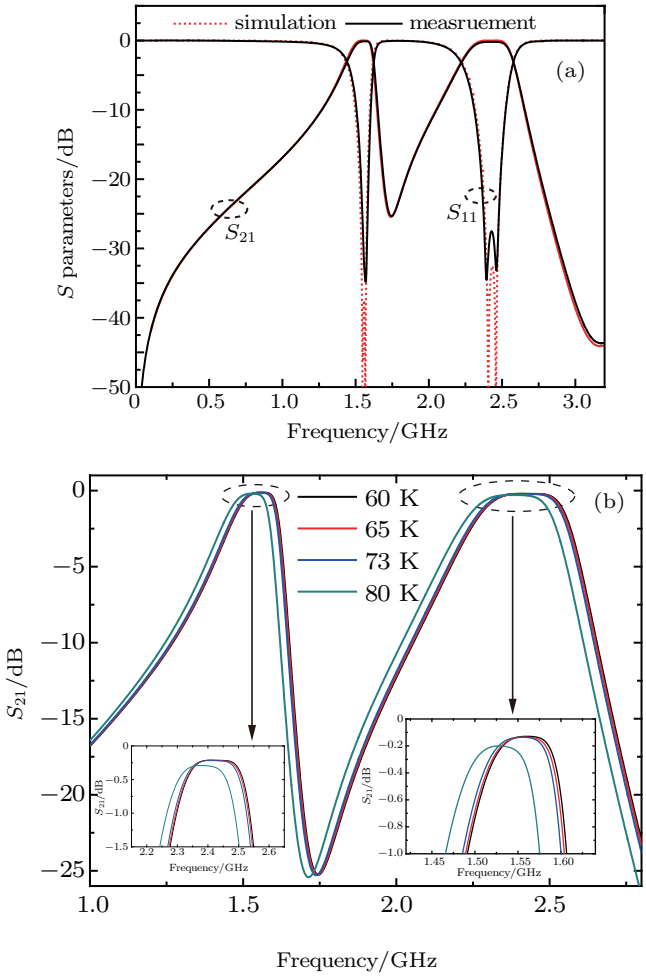


Fig. 7. (color online) (a) Simulated and measured results of the dual-band filter, (b) values of measured S_{21} transmission coefficient of dual-band filter at various operating temperatures.

The final layout of the dual-band filter and its coupling structure are shown in Figs. 6(a) and 6(b), respectively. Each band of the filter is designed using the parallel-coupled microstrip line method. Stubs 1 and 2 constitute the high band

centered at 2.44 GHz, while Stubs 1′ and 2′ the low band centered at 1.53 GHz. The two bands share one patch. The simulation result of lossless transmission line is shown in Fig. 7, and the entire circuit size is 9.5 mm×8.9 mm (approximately $0.15\lambda_g \times 0.14\lambda_g$), where λ_g is the guided wavelength of the low-band frequency.

4. Fabrication and measurement

The single- and dual- band filters were both fabricated on a 0.5-mm-thick MgO substrate with double-sided 600-nm YBCO HTS films and then assembled as shown in Fig. 8. These filters were measured at 70 K by an Agilent Network Analyzer. The measured results of the single-band filter are related to the simulated results and the center frequency is 6.02 GHz with a 25.6% FBW as shown in Fig. 3. This filter exhibits a return loss and a low insertion loss better than 13.5 dB and 0.04 dB, respectively. As shown in Fig. 7(a) the two measured passbands of the dual-band filter are centered at 1.53 GHz and 2.44 GHz with FBWs of 12.1% and 14.1%, respectively. The maximal in-band insertion losses are 0.12 dB and 0.20 dB, and the return loss is better than 25 dB in both passbands. The measured results agree well with the simulated results. Besides, as shown in Fig. 7(b), when temperature is changed from 60 K to 80 K, the insert loss increases and the passband shifts to a lower frequency. The bandwidth decreases slightly as well. It is evident that a higher temperature will enhance the surface resistance. In addition Table 2 shows a comparison of the results of this work with the reported results of dual-band filters.

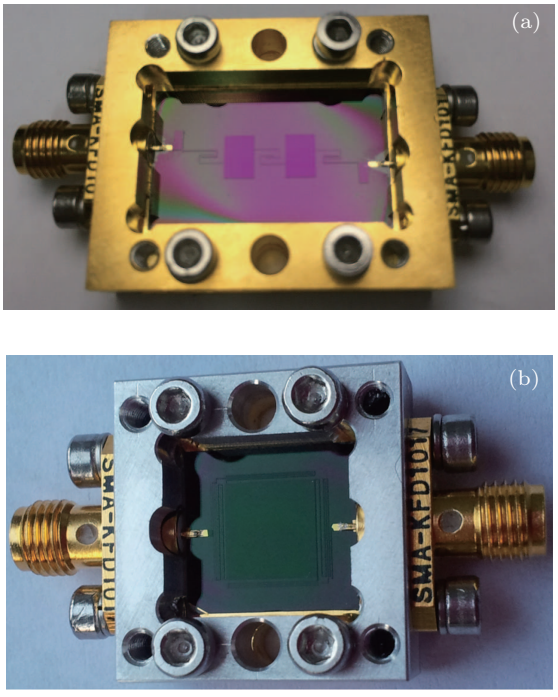


Fig. 8. (color online) Photographs of the fabricated HTS (a) single-band and (b) dual-band filters.

Table 2. Comparison between the proposed dual-band filter and others.

	f/GHz	FBW/%	$\lvert S_{11}\rvert$/dB	$\lvert S_{21}\rvert$/dB	Size ($\lambda_g \times \lambda_g$)
Ref. [5]	0.8/2.0	2.0/2.0	13.5/12.5	0.25/0.08	0.21×0.19
Ref. [16]	1.91/5.44	66.7/28.3	15/17	0.3/0.5	0.21×0.13
Ref. [17]	2.5/3.5	6.9/3.8	16/16	0.3/0.33	0.47×0.24
This work	2.44/1.53	12.1/14.1	25/35	0.12/0.20	0.15×0.14

5. Conclusions

Transmission zeroes can be generated by two or more DSIRs to improve the out-of-band rejection of a single-band filter. The proposed QSIR can be used to design a dual-band filter with independent and controllable frequencies. A dual-band filter with the characteristics of compact size, good performance, and high design freedom is achieved in this work. For future work, the QSIR can be used to introduce transmission zeroes outside the two passbands, which can improve the rejection between the two bands.

References

[1] Chen F, Hao J, Li H G and Cao Z Q 2011 *Acta Phys. Sin.* **60** 74223 (in Chinese)
[2] Zhang Q S, Zhu F J and Zhou H S 2015 *Chin. Phys. B* **24** 107506
[3] Guan X H, Peng Y, Liu H W, Lei J H, Ren B P, Qin F, Wen P, Liu F and Liu Y D 2016 *IEEE Trans. Appl. Supercond.* **26** 1501905
[4] Liu X Y, Zhu L and Feng Y J 2016 *Chin. Phys. B* **25** 034101
[5] Sekiya N 2016 *IEEE Trans. Appl. Supercond.* **27** 1501104
[6] Zuo T, Zhao X J, Wang X K, Yue H W, Fang L and Yan S L 2009 *Acta Phys. Sin.* **58** 4194 (in Chinese)
[7] Wang X, Wei B, Zheng T N, Cao B S, Jiang L N and Chen J B 2016 *Physica C* **531** 9
[8] Xu E M, Zhang Z X and Li P L 2017 *Chin Phys. Lett.* **34** 014203
[9] Sun L and He Y S 2014 *IEEE Trans. Appl. Supercond.* **24** 1501308
[10] Ohshima S 2000 *Supercond. Sci. Technol.* **13** 103
[11] Zhang X, Liu J P, Yan S L, Fang L, Zhang B and Zhao X J 2015 *Supercond. Sci. Technol.* **28** 065016
[12] Zhang T L, Yang K, Zhu H, Zhou L G, Jiang M Y, Dang W, Ren X Y and Hou F Y 2015 *Supercond. Sci. Technol.* **28** 105012
[13] Gao T, Wei B and Heng Y 2017 *Chin. Phys. B* **26** 058503
[14] Liu A S, Huang T Y and Wu R B 2008 *IEEE Trans. Microw. Theory Tech.* **56** 2921
[15] Chin K S and Yeh J H 2009 *IEEE Microw. Wireless Compon. Lett.* **19** 155
[16] Xu J, Ji Y X, Miao C and Wu W 2013 *IEEE Microw. Wireless Compon. Lett.* **23** 338
[17] Lu X L, Wei B, Cao B S, Guo X B, Zhang X P, Song X K and Heng Y 2014 *IEEE Trans. Appl. Supercond.* **24** 1500205
[18] Liu H W, Li S and Ren B P 2013 *Electron. Lett.* **49** 887
[19] Hong J S, Hussein S and Chun Y H 2007 *IEEE Trans. Microw. Theory Tech.* **55** 1764
[20] Hong J S 2011 *Microstrip Filters for RF/microwave Applications*, 2nd. edn. (New York: Wiley)